Acoustic simulations in Spherical Geometry: Can we detect convection?

S. M. Hanasoge

W. W. Hansen Experimental Laboratory, Stanford University, Stanford, CA 94305

T. L. Duvall, Jr.

Laboratory for Solar and Space Physics NASA/Goddard Space Flight Center, Greenbelt, MD 20771

M. L. DeRosa

Lockheed Martin, Palo Alto, CA

M. S. Miesch

HAO, NCAR, Boulder, CO

shravan@stanford.edu

ABSTRACT

We investigate the possibility of detecting convection by computing traveltime shifts caused by wave propagation through the convection zone. The convection zone is modeled using a snapshot from an Anelastic convection simulation. We present results obtained from a ray calculation of traveltime shifts. We also discuss the state of art in acoustics simulations in spherical geometry and present the latest results.

1. Introduction

Considerable effort has gone into the possibility of detecting convection, with the earliest efforts focused on being able to see giant cells. Recently, Swisdak & Zeibel (1999) have attempted to detect changes in the solar eigenfrequencies caused by large scale convective motions. Giant cells have never been seen conclusively and there has been no clear detection of sub-surface convective activity. In this article, we apply the method of time-distance helioseismology (Duvall et al. 1993) to determine if the traveltime shifts induced by a model of solar convection in waves propagating through this convective field are detectably large. Traveltime calculations using solar data are currently being performed using the deep-focusing technique described in Jensen et al. (2003). We also discuss the applications of the simulational procedure developed to compute the solar acoustic wavefield (see Hanasoge et al. (2005), Hanasoge (2006)).

2. Ray calculations

We use a standard method to compute traveltimes caused by the interaction of acoustics with a flow-field (for example, see Giles 1998). The traveltime shift, $\delta\tau$, is given by

$$\delta\tau = 2\left[\int_{r_1}^{r_2} \frac{u_h}{c^2}\left(\frac{\omega^2 r^2}{l(l+1)} - c^2\right)^{-\frac{1}{2}} dr + \int_{r_1}^{r_2} \frac{u_r}{c^2} dr\right], \tag{1}$$

where r is the radius, u_h is the horizontal flow velocity in the direction of the propagating ray, u_r is the radial velocity, ω the frequency of the acoustic wave, l the spherical harmonic order, c the sound speed, r_1 the lower turning point and r_2 is the upper turning point. The first and second terms on the right-hand-side denote traveltime contributions from the horizontal and radial components of the flow, respectively. For the calculation presented here, a ray with $l = 105$, $\nu = 3.2$ mHz, and inner turning point at $r_t = 0.89R_\odot$, was propagated through the velocity field.

2.1. Convection model

The Anelastic Spherical Harmonic (ASH) code (Miesch et. al. 2000) computes acoustics-free convection in a spherical shell. For the simulation used in the current calculation, the computational boundaries were placed at $0.76R_\odot$ and $0.93R_\odot$ and act as no-slip walls. Because of the wall-like boundary conditions, convection comes to a halt at both ends and it is important to keep this aspect in mind while interpreting the results from the ray calculations. In reality, acoustic signals are strongly biased by the near-surface supergranular activity. In order to take this effect in account, the supergranules are modeled by cell-like structures with an average horizontal cellular size of 30 Mm. Each unit acts a 'convective cell', with velocity profiles chosen to satisfy the continuity equation, $\boldsymbol{\nabla}\cdot\mathbf{v} = 0$ (for example, see Swisdak & Zeibel 1999). The surface velocity profile and a vertical cut are shown in Figure 1. We also mention that the ASH profile used for this calculation has large cyclonic features that persist through the entire simulation domain.

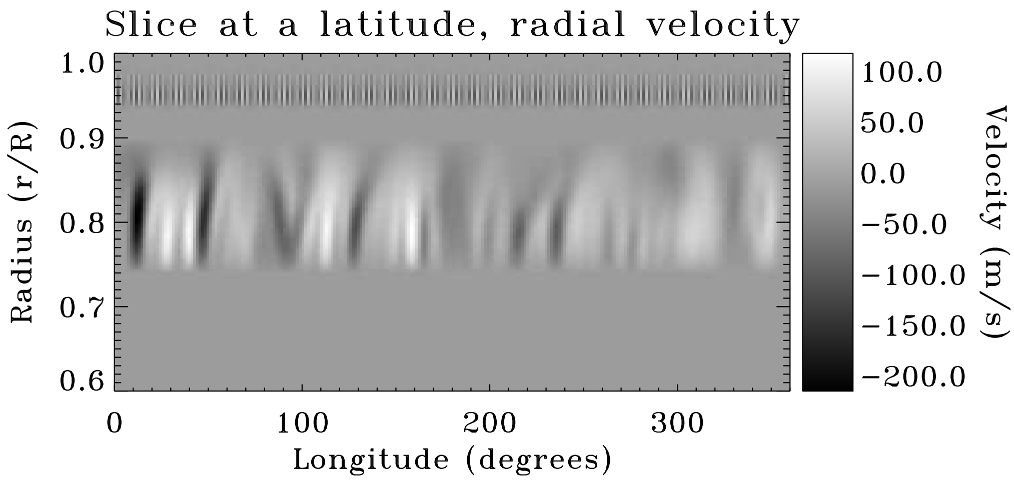

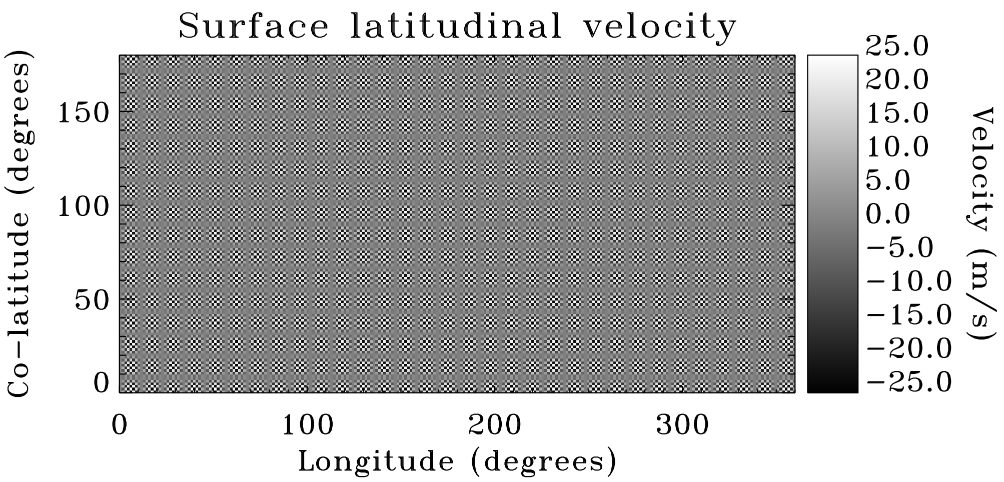

Fig. 1.— Sections of velocity profiles. The upper panel shows a radial cut at a single latitude of the radial velocity. Notice that the convection in this case extends from about $0.76R_\odot$ upto $0.93R_\odot$. The uppermost layers are represented by an artificial 'convection' profile. In the lower panel, a surface view of the cellular 'supergranular' structure is visible.

2.2. Traveltimes and correlation

The center to annulus averaged north-south and east-west traveltimes have been computed and are shown in Figure 2. At the inner turning point radius of the ray, correlations of the longitudinal velocity with the east-west traveltimes and the latitudinal velocity with the north-south traveltimes are computed. These are shown in Figure 3. The average rms east-west traveltime shift produced by the convection profile is 2.06s, and the average rms north-south traveltime shift is 1.73s. The largest traveltime shifts we observe are of the order of 7s. The maximum correlation between the velocity profiles and the corresponding traveltime maps is very high, 0.87 for the north-south map with the latitudinal velocity (at the inner turning point) and 0.77 for the east-west map with the longitudinal velocity.

3. Acoustic simulations in spherical geometry

The computational and validation procedures employed in the simulation of acoustic wave propagation in spherical geometry may be found in Hanasoge et al. (2005). In the past, we had encountered the difficulty of the atmosphere being convectively unstable, leading to exponentially growing instabilities. The e-folding timescales of the instability lie in the range of 5 minutes to several hours. To compute the acoustic wave-field in a finite amount of time, we solve the Euler equations in the linear limit, and therefore the capability to model the essentially non-linear convective physics is not present. Consequently, unchecked by the non-linear terms, the instabilities created by the inherently unstable background state grow with time, eventually destroying the accuracy of the simulation altogether.

To circumvent this problem, we devised an atmosphere that closely resembles the atmosphere described model S of the sun (Christensen-Dalsgaard et al. 1996), but is convectively stable. Quite importantly, the reflective properties of this alternate atmosphere are almost identical to that of model S. The details of this atmosphere may be found in Hanasoge (2006). Using this model of the atmosphere, coupled with model S of the interior, we present results from a 24 hour long simulation. The computation was completely stable with no signal corruption due to the fast growing instabilities in the outer layers. We show the log power spectrum obtained from this simulation in Figure 4. The band like structure in frequency visible between 2 - 5.2 mHz is due to the restricted nature of the excitation spectrum. We are uninterested in frequencies below 2 mHz and above 5.5 mHz and consequently do not excite any modes in that region.

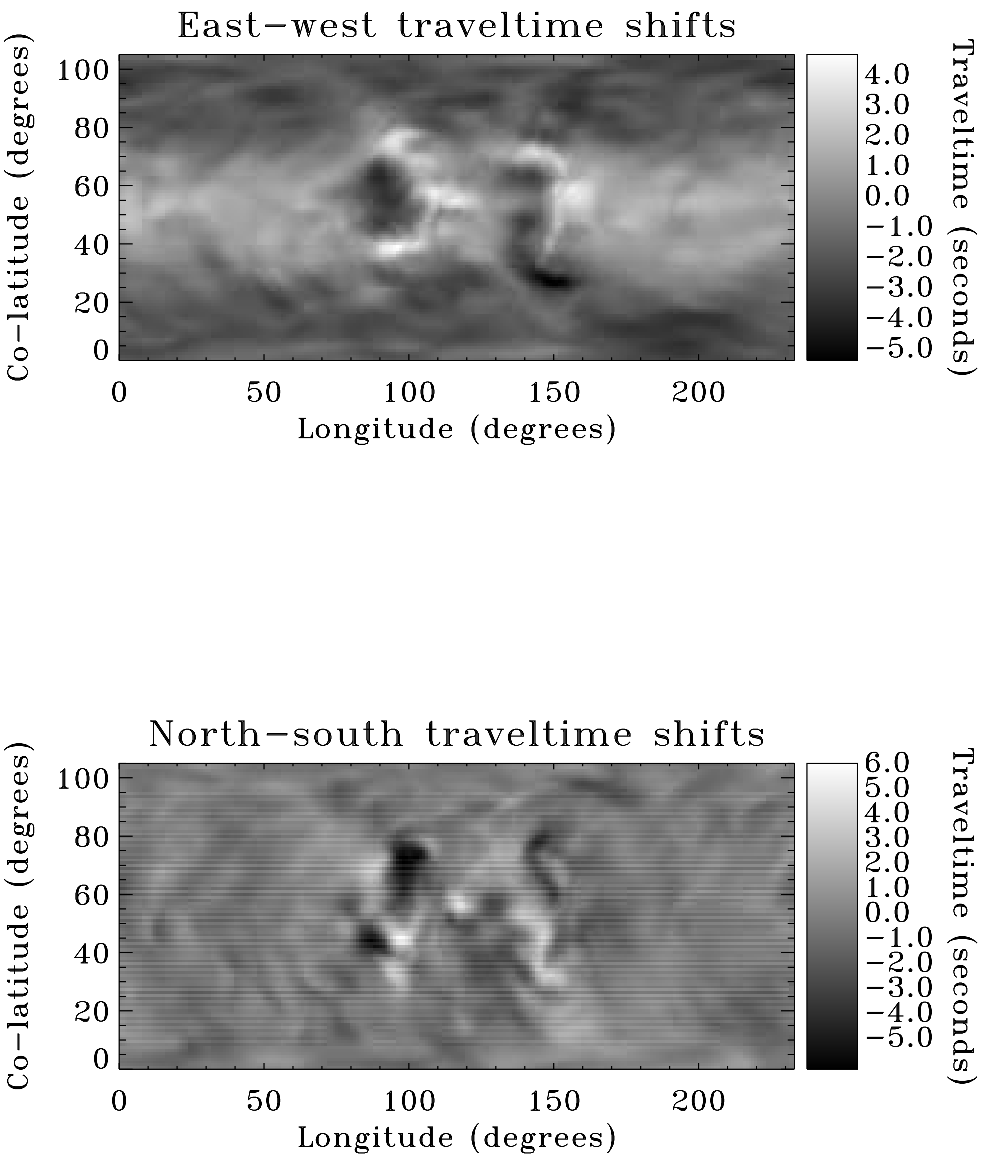

Fig. 2.— Center to annulus traveltime shifts accumulated by acoustic wave propagation through an ASH convection profile coupled with an artificial supergranulation profile, seen in Figure (1). A ray with $l = 105$, $\nu = 3.2$ mHz, and inner turning point at $r_t = 0.89 R_\odot$, was propagated through the velocity field to compute the traveltime shifts.

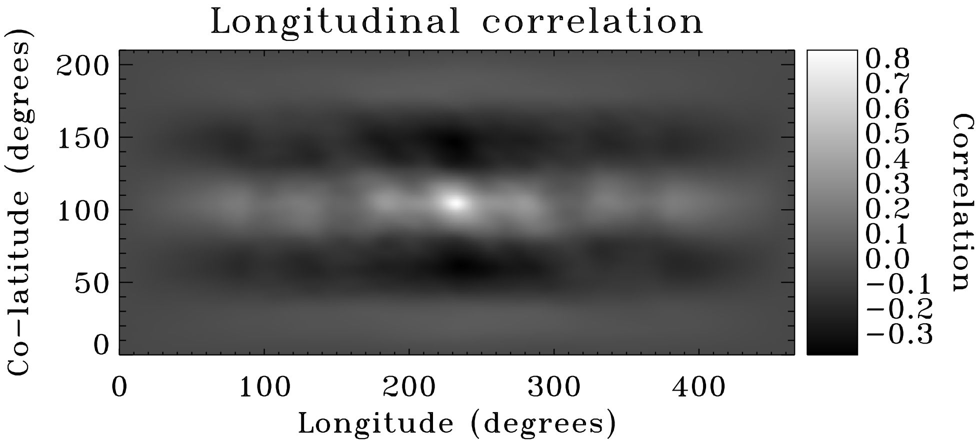

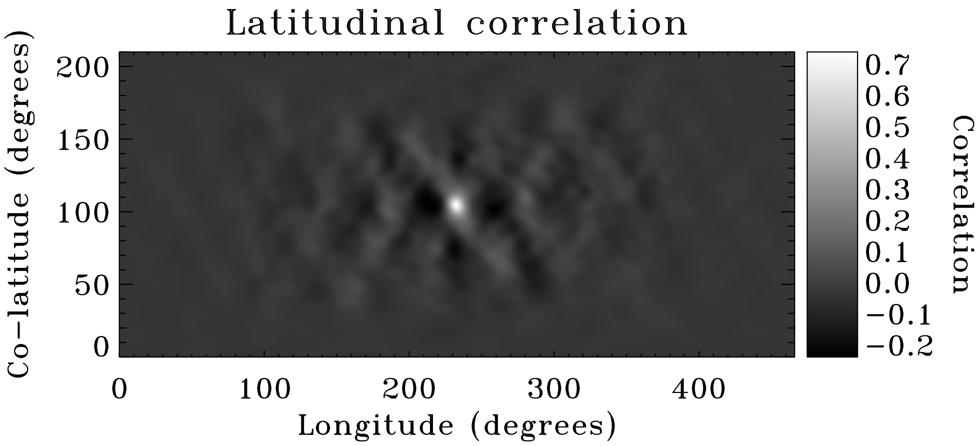

Fig. 3.— Correlation maps between traveltimes and corresponding velocities. In the upper panel, accumulated east-west traveltime shifts are correlated with the longitudinal velocity profile (the profile at the inner turning point of the ray). The lower panel shows a similar metric, but in this case, the accumulated north-south traveltime shifts are correlated with the latitudinal velocity profile (the profile at the inner turning point of the ray). It is interesting to note that the maximum correlation is very high, of the order of 0.87 for longitudinal correlations, and 0.77 for the latitudinal counterpart.

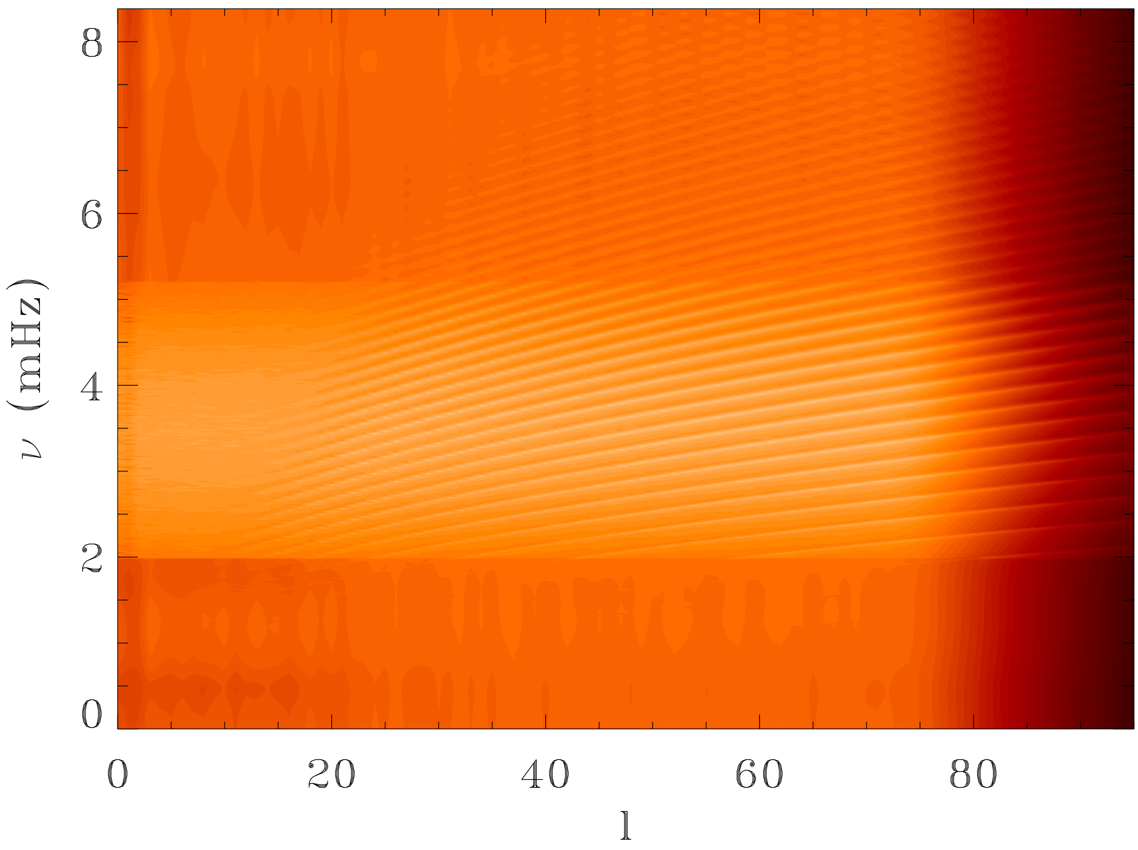

Fig. 4.— Log power spectrum of a 24 hour long acoustic simulation. The computational boundaries are located at $0.22R_\odot$ and $1.0002R_\odot$. The lower boundary acts as a phase speed filter, removing all waves whose turning points lie below the lower boundary. The highest spherical harmonic order in this simulation was $l_{max} = 96$. The band like structure in frequency visible between 2 - 5.2 mHz is due to the restricted nature of the excitation spectrum. We are uninterested in frequencies below 2 mHz and above 5.5 mHz and consequently do not excite any modes in that region.

REFERENCES

Christensen-Dalsgaard, J., et al. 1996, Science, **272**, 1286

Duvall, T. L., Jefferies, S. M., Harvey, J. W., & Pomerantz, M. A. 1993, Nature, 362, 430

Jensen, J. M., Duvall, T. L., Jr., Bo Holm J. 2003, proceedings of SOHO12, 315

Giles, P. M., Ph.D thesis, Stanford University, 1998

Hanasoge, S. M. et al., submitted to ApJ, 2005

Hanasoge, S. M., to appear in the ILWS conference proceedings, 2006

Miesch, M. S., Elliott, J. R., Toomre, J., Clune, T. L., Glatzmaier, G. A., Gilman, P. A., ApJ, 532, 593-615

Swisdak, M. & Zeibel, E. 1999, ApJ, **512**, 442